

LiPro: light-based indoor positioning with rotating handheld devices

Bo Xie^{1,2} · Shimin Gong² · Guang Tan² 

© Springer Science+Business Media New York 2016

Abstract In this paper, an indoor positioning method, namely LiPro, is proposed for handheld devices such as smartphones. Based on an empirical light intensity model, we propose a rotating multi-face positioning method that enables a receiver to locate itself in ill-conditioned scenarios which would otherwise make the traditional multi-lateration impossible—for example when less than three LED lamps are visible to the receiver. In this method, the user manually performs three rotations of the receiver around three orthogonal axes, in a manner similar to the calibration process of a compass. During this process, the receiver continuously collects RSS and magnetic field strength, which are then used to solve for the receiver's position. LiPro can work with a single source of light, making it a more cost-effective and less demanding than previous approaches. Our experiments show that LiPro achieves a median error of 0.59 m in a corridor with linearly deployed LEDs, and 0.45 m in an office. Moreover, LiPro is shown to be robust against interference from ambient light sources.

Keywords Indoor positioning · LED light · Rotation

1 Introduction

Location-based services (LBS) and applications, relying on the positioning capability of mobile devices, have been studied extensively over the past decade, especially with

the recent boom of Internet of Things. Accurate indoor positioning opens opportunities for a wide range of applications, such as personal navigation, object search, and robot control. Although the GPS provides satisfactory positioning performance in outdoor scenarios, it does not work indoors due to the blockage of satellite signals [15]. To address this problem, researchers have explored various techniques such as radio frequency (RF), ultrasound, magnetism, and light to enable indoor positioning. Due to interference and the multipath effects, RF based approaches normally produce accuracy to a few meters. Light-based approaches improve on this by leveraging the better predictability of light propagation, at the cost of reliance on line of sight between the transmitter and receiver.

In light of the widely deployed LEDs in indoor environments, such as airport terminals, warehouses, and hospitals (see Fig. 1), we propose the LiPro method that uses the built-in light sensor of a handheld device, referred to as the *receiver*, for positioning. A light sensor is a type of photodiode with a PN or PIN structure, and is capable of sensing incident light and outputting intensity readings. The received light intensity, or received signal strength (RSS), is a function of the distance and angles between the LED and the receiver. Assuming known positions of the LEDs, the position of the receiver can potentially be derived from RSS and geometric constraints.

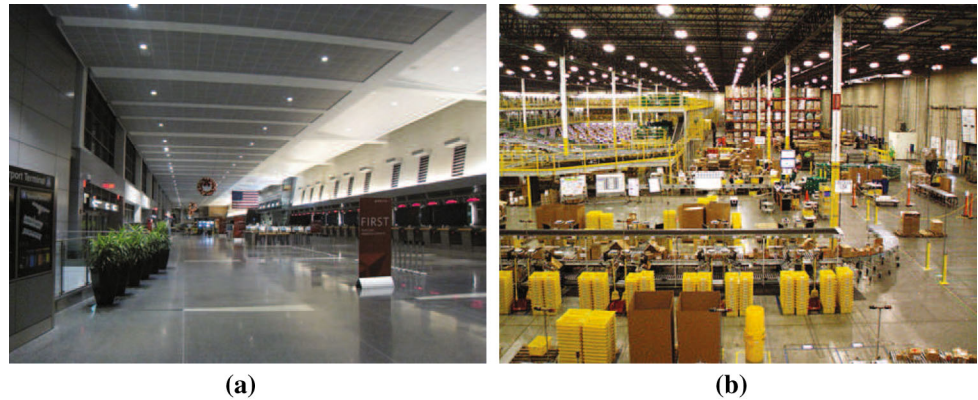
We first establish an RSS model based on the Lambertian radiation pattern [2]. The model characterizes the attenuation of light intensity over space with three independent parameters: distance between the lamp and receiver, radiation angle from the LED and incident angle on the sensor. To avoid interference between nearby LEDs, we design the modulation scheme, optical channel allocation policy, and the structure of beacon frames. We propose a *rotating multi-face positioning* (RMFP) method that

✉ Bo Xie
bo.xie@siat.ac.cn

¹ University of Chinese Academy of Sciences, Beijing, China

² SIAT, Chinese Academy of Sciences, Shenzhen, China

Fig. 1 LEDs in **a** an airport terminal and **b** a warehouse



enables the receiver to position itself. In this method, the user rotates the receiver around the three axes, x , y and z in her body coordinate system, during which course the receiver continuously collects RSS values. At the same time the receiver also measures magnetic field strength to correct the heading measurement [22]. We show how to select particular measurements to form a set of constraints that allow us to find a unique solution of the receiver's position. The main highlight of the RMFP method is that it makes positioning possible with only a single lamp in sight of the receiver. This dramatically reduces the system's dependence on a high density of lamp deployment compared with the conventional multilateration approach.

We have implemented a prototype system and conducted experiments in two settings. In the first setting, the lamps are sparsely deployed along a line in a corridor, where the traditional multilateration method fails. LiPro successfully produces position results with a median error of 0.59 m. In an office area with three nonlinear lamps in sight, LiPro is able to produce positions with a media error of 0.45 m. Moreover, LiPro is robust against interference from ambient light sources.

2 Related work

There is a large body of literature on indoor positioning techniques, mostly based on a fingerprint database or ranging techniques. Given the ubiquitous radio frequency (RF) signals, measurement of RSS of WiFi [1, 5, 28, 32], cellular radios [24], or FM radios [4], can be used to build an RF signature database, or to establish a signal propagation model for positioning. However, RF signal is susceptible to noise and interference, and thus is highly unstable, leading to rather coarse-grained positioning results, with distance errors typically to a few meters [23]. Hence, many efforts have been devoted to mitigate the instability in a multi-path fading environment [8, 12, 21, 27]. In a densely

deployed network, the multi-path effect is leveraged to achieve improved positioning accuracy for RFID tags [26]. A similar technique is implemented in the RF-compass system [25]. Another RF-based ranging technique is to estimate the signal's angle of arrival (AoA) [13, 14], which may require sophisticated hardware design and signal processing algorithms. Arraytrack [28] achieves sub-meter accuracy by employing antenna arrays, and so does Ubicarse [9]. Tagoram [29] constructs an RF phase hologram to localize a moving RFID tags.

In contrast to RF signals, light signal is much less affected by the multi-path effect, and thus is viewed as an appealing approach to accurate indoor positioning. Many proposals in this domain have considered the multi-lateration method [2, 30, 31, 34]. Rajagopal et al. [19] use the LED as the reference point and exploit the rolling shutter effect of camera sensor. A similar idea has been adopted by the commercial project ByteLight [3]. Epsilon [11] relies on the measurements of light intensity from at least three LEDs and adopts the conventional multi-lateration method for positioning. Under ideal conditions, it reports position accuracy to about a half meter. However, when Epsilon operates in an ill-conditioned environment with only one or two LEDs available, the performance is severely compromised. To further improve positioning accuracy, a hybrid RSS/AoA method is proposed in [17]. By using AoA estimation from image analysis, Luxapose [10] achieves accuracy to around 10 cm. This approach, however, depends on a very dense deployment of lights which incur a high cost.

Chung et al. [6] propose a method that locates the receiver by exploiting the geomagnetic field, which is similar to the RF fingerprint approach. Technologies with accurate ranging, such as the ultra wide band (UWB) [20] or the combination of radio and sound signals [18], can improve positioning accuracy, but are generally expensive to deploy. Yun et al. [33] propose to use the frequency

shifts of sound to enable device tracking, with around 1.4 cm tracking accuracy.

3 The RSS model

In this section, we establish the RSS model which lays the foundation for our positioning method. First we describe how to measure RSS, taking into account environmental interference, and then we empirically determine the parameters of the model.

3.1 Avoiding interference

The RSS of light is generated by the light sensors at the receiver. In practice, there exist environmental lights such as sunlight and artificial lights, so the sensed light is a mixture of multiple components. To obtain the intensity from a particular LED, we let the LED flash at a specified frequency under the control of a micro-controller. This will generate a sequence of square waves. We denote the light intensity by a periodical function $f(t)$, as shown in Fig. 2. For simplicity, let the square wave $f(t)$ have a duty cycle of 50%, and thus the fourier series expansion of $f(t)$ is

$$f(t) = \frac{E}{\pi} \sum_{n=1}^{\infty} \frac{1 - \cos(n\pi)}{n} \sin\left(n \frac{2\pi}{T} t\right), \tag{1}$$

where $n = 1, 2, 3, \dots$ denotes the harmonic orders, and E is the received light intensity when the LED source is turned on. The coefficients of the fourier series represent the signal energy on different harmonics. Note that the first harmonic frequency equals the flicker frequency $1/T$, while the higher order harmonics are multiple times of the

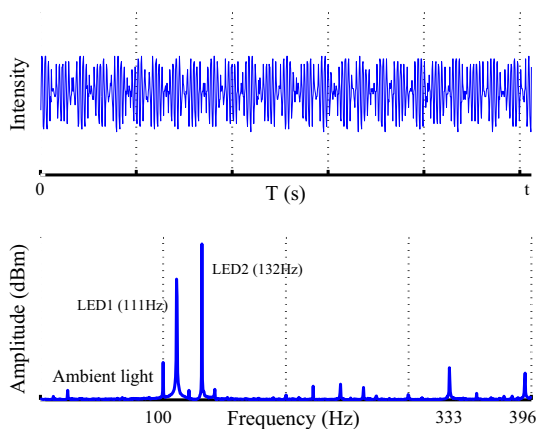


Fig. 2 RSS in the time and frequency domains excluding the DC component. The first harmonics of the light carriers of the two LEDs are 111 and 132 Hz

first harmonic frequency and the strengths on even order harmonics are zeros. Equation (1) indicates that the total energy of the received LED light is scattered over different harmonics. Though it is impractical to extract the light energy from all harmonics, we find that the energy of the first harmonic (i.e., $2E/\pi$) is proportional to the received light intensity E and irrelevant to the flicker frequency $1/T$. Therefore, by performing the fourier transformation of $f(t)$ and measuring the strength of the first harmonic, the receiver can determine the light intensity.

3.2 Establishing the model

We assume that the LED lamp is mounted on the ceiling with the LED chip facing vertically downward. The light intensity sensed by a light sensor from an LED is impacted by three factors: the distance d between the LED and the receiver, the radiation angle ω from the LED, and the incident angle μ , as illustrated in Fig. 3. Define the *central ray* as a ray extending straight downward from the LED chip. Thus, ω is the angle between the incident ray and the central ray, and μ is the angle between the incident ray and the normal vector of the surface of the light sensor, or the sensing plane.

The impacts of d , μ and ω on the RSS s are denoted by $f_d(d)$, $f_\mu(\mu)$, and $f_\omega(\omega)$, respectively. Thus, s is a function of d , μ and ω :

$$s(d, \mu, \omega) = f_d(d) \cdot f_\mu(\mu) \cdot f_\omega(\omega). \tag{2}$$

To simplify the representation (2), we visualize a Cartesian coordinate system as depicted in Fig. 3. The light sensor and the LED are centered at the origin $(0, 0, 0)$ and (x, y, z) , respectively. The distance between the LED and the receiver is $d = \sqrt{x^2 + y^2 + z^2}$. Let (A, B, C) denote the

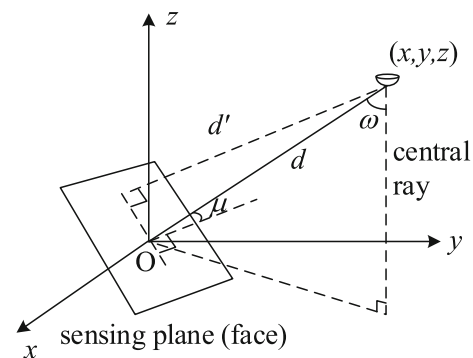


Fig. 3 The light intensity model: the light sensor and the LED are located at $(0, 0, 0)$ and (x, y, z) , respectively. The received light intensity s relates to the distance d , incident angle μ , and radiation angle ω

normal vector of the sensing plane. Then, the distance from the LED to the sensing plane is given by

$$d' = \frac{|Ax + By + Cz|}{\sqrt{A^2 + B^2 + C^2}}.$$

Now, we can determine the incident angle μ and the radiation angle ω as follows:

$$\mu = \arccos(d'/d),$$

$$\omega = \arccos(z/d).$$

Putting all terms together, we can evaluate the light intensity as

$$s(x, y, z) = \frac{k}{d^2} \cdot f_\mu\left(\arccos\left(\frac{d'}{d}\right)\right) \cdot f_\omega\left(\arccos\left(\frac{z}{d}\right)\right). \quad (3)$$

where $k > 0$ is a constant light intensity.

We conduct experiments in three settings. In the first setting, we fix $\mu = 0^\circ$ and $\omega = 0^\circ$, and gradually increase d from 1 to 6 m while measuring the light intensity as shown in 5(a). The results confirm the inverse-square law, that is, $f_d(d) = k/d^2$, see Fig. 4(a). The coefficient k corresponds to the light intensity measured at $d = 1$ m. In the second setting, we keep $\omega = 0^\circ$ and d unaltered, and then vary the incident angle μ from 0° and 90° by tilting the receiver (and the sensing plane at the same time) as illustrated in Fig. 5(b). The normalized measurements are shown in Fig. 4(b). We observe that, the angular function $f_\mu(\cdot)$ for different distance d are almost in the same form, indicating that the decomposition in (3) is reasonable. In the third setting, by varying the radiation angle ω as shown in Fig. 5(c), we record the normalized measurements in Fig. 4(c). For each setting, we perform curve fitting and obtain closed-form expressions for $f_d(\cdot)$, $f_\omega(\cdot)$, and $f_\mu(\cdot)$, respectively. The established light intensity model is robust as all the results are obtained in an office environment with multiple sources of ambient light.

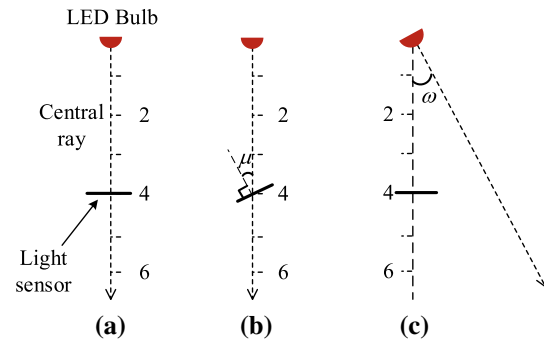


Fig. 5 Three measurement settings

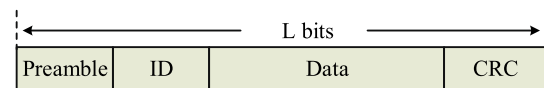


Fig. 6 Beacon frame

4 LED data communications

The LED lamp needs to broadcast its location and RSS model parameters to the receiver. The data is carried in a periodic beacon frame, which is divided into a few fields: frame preamble, LED ID, data, and CRC, as shown in Fig. 6.

The preamble is known to the receiver and serves as a synchronization code to determine the starting point of the beacon frame. It is also the energy signal, that is, the receiver can sample the preamble and perform the fourier transformation to extract the light intensity on the 1st harmonic frequency, which serves as an estimate of the received light intensity.

4.1 BFSK modulation

The data carried in the beacon frame is coded into a binary bit stream and then modulated by the LED's flicker pattern to avoid interference with ambient lights. The duration of

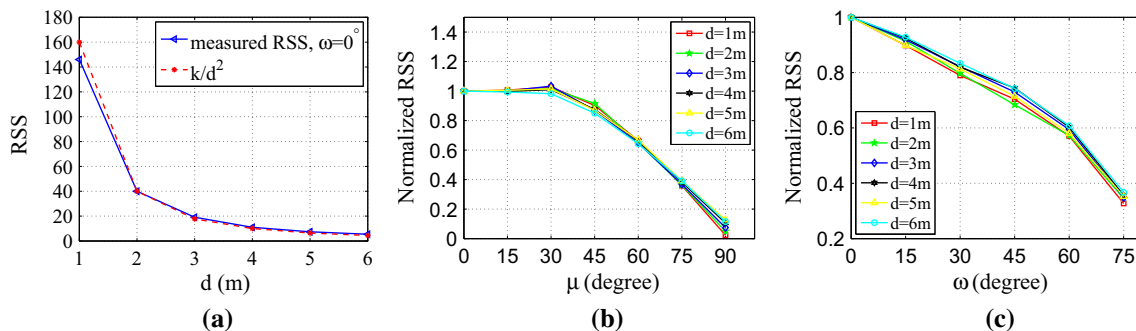


Fig. 4 The light intensity as a function of d , μ , and ω . **a** $f_d(d)$, **b** $f_\mu(\mu)$, **c** $f_\omega(\omega)$

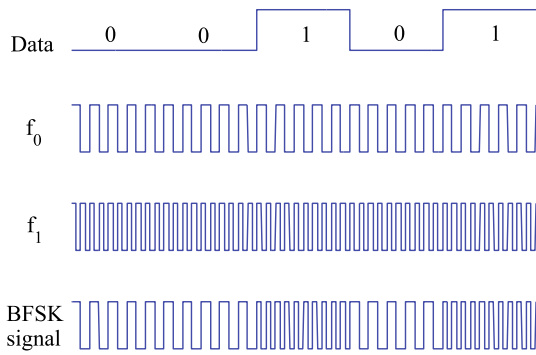


Fig. 7 BFSK modulation: the binary information “0” and “1” are modulated by two square waves with different frequencies f_0 and f_1 , respectively

each information bit lasts a symbol length. There are many modulation schemes, such as PSK, ASK, and BFSK, proposed for visible light communications. Some of these schemes require complex algorithms or special hardware to modulate/demodulate the bit stream.

In this work, we adopt the BFSK scheme for its simplicity, as illustrated in Fig. 7. The modulation relies on the off-the-shelf micro-controller that switches the LED source between the “ON” and “OFF” states. The switching of LED states is controlled at two different frequencies f_0 and f_1 , representing the symbols “0” and “1”, respectively. At the receiver, time-domain sampling of the sensed light intensity in a symbol length is transformed into frequency domain. Then we can inspect on the frequency components and make binary decisions to determine the information bit carried in the beacon frame.

4.2 Optical channel allocation

When multiple, unsynchronized light sources broadcast beacons over shared light medium, at the receiver side, the beacons may interfere with each other or with ambient lights. It is infeasible to adopt time division multiple access (TDMA) to coordinate among the light sources since they are not designed to communicate with each other. We channelize the whole available bandwidth of light medium into multiple disjoint and even-spaced sub-carriers; two adjacent sub-carriers comprise one subchannel. In LiPro, we choose to allocate a static subchannel to each light source. However, in indoor scenario with large space, there is a possibility that the number of subchannels is less than the number of light sources deployed. In this case, we spatially separate the subchannels for nearby LEDs to avoid collision.

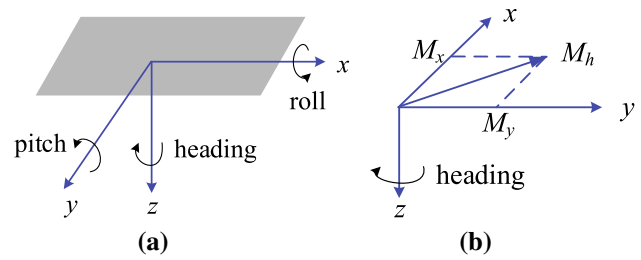


Fig. 8 **a** Aircraft body coordinates and **b** heading calculation

5 Normal vector calculation

In this section, we describe the calculation of the normal vector based on a 3-axis magnetic sensor and a 3-axis accelerometer. Following the aircraft convention, we need to determine three angles, namely the *pitch*, *roll* and *heading*, as shown in Fig. 8(a). Once the attitude angle of the receiver is determined, we can calculate the normal vector (A, B, C) of the sensing plane.

5.1 Attitude angle measurement

The *pitch* and *roll* can be calculated as

$$\text{pitch} = \arcsin(-A_x),$$

$$\text{roll} = \arcsin(A_y / \cos(\text{pitch})),$$

where A_x and A_y are the normalized measurements of the gravity imposed on the x and y axes of the accelerometer, respectively. Figure 9 shows that the measurement error is less than 2° . The measurements of *heading* is provided by the magnetic sensor:

$$\text{heading} = \arctan(M_y / M_x),$$

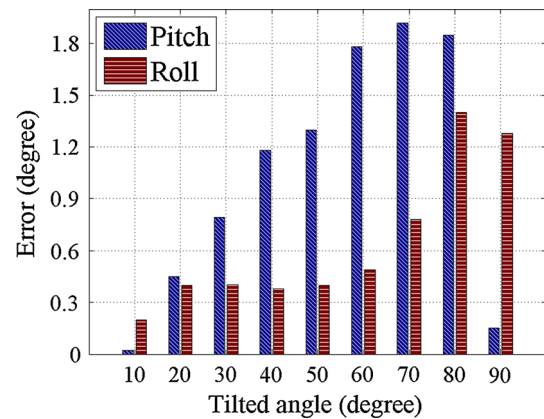


Fig. 9 Measurement errors of pitch and roll

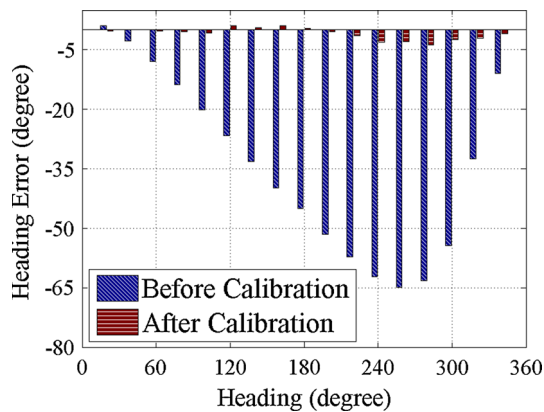


Fig. 10 Measurement errors of heading produced before and after applying the ellipsoid calibration

where M_x and M_y are the strengths of magnetic field on the x and y axes of the magnetic sensor, as illustrated in Fig. 8(b) where M_h is the horizontal component of the earth’s magnetic field pointing to the magnetic North Pole.

5.2 Magnetic sensor calibration

In practice, the magnetic sensor is susceptible to the interference from ambient magnetic fields, resulting in great errors. Figure 10 shows that the heading error can be up to 60° , which will severely decrease the positioning accuracy.

A magnetic sensor may experience varying distortion patterns at different locations, thus calls for a method to correct the measurement. In our work, we adopt the *three-axis rotation* method to do this. In this method, the user rotates the receiver around the three axes, x , y and z in the body coordinate system, see Fig. 11. Ideally, the normalized magnetometer measurements should lie on the surface of a sphere centered at the origin. However, due to magnetic interference, the distribution of the measurements will deviate from the sphere, as shown in Fig. 12(a). We

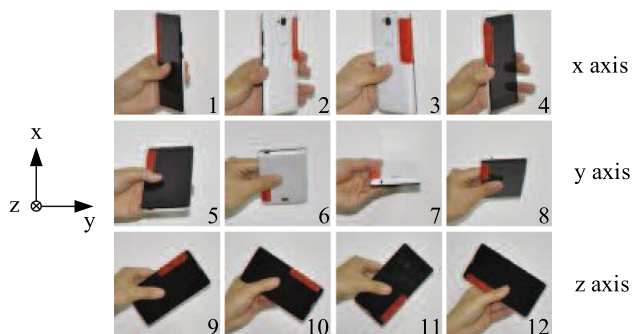


Fig. 11 A top view of the rotating receiver (smartphone) at a fixed position

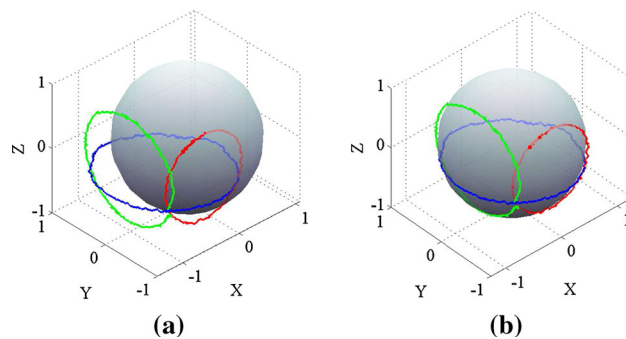


Fig. 12 Measurements before and after magnetic sensor calibration. **a** Three circles deviating from the sphere. **b** Results after calibration

adopt the ellipsoid calibration method [16, 22] to calibrate the magnetic sensor. The calibration parameters of ellipsoid can be calculated by using the least square method. Figure 12(b) indicates that the corrected measurements now are well distributed on the sphere. Figure 10 shows the heading error drops to around 4° .

6 Rotating multi-face positioning

With the RSS model and all system parameters collected, one can naturally choose to position the receiver via the classic multilateration method. However, such a method requires at least three nonlinear lamps being visible to the receiver. This may not be satisfied in many practical situations, for example in a corridor where the lamps are deployed on a line, or when the light is blocked by furniture or the user herself.

To address this problem, we propose a rotating multi-face positioning method that can work with only a single visible light source. This method takes advantage of the *three-axis rotation* process that has been exploited to

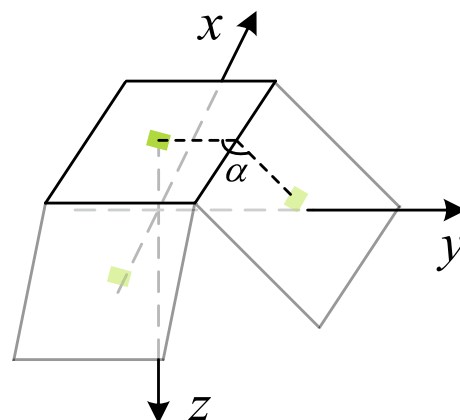


Fig. 13 Three sensing planes generated at a fixed position; the light sensor is represented by a green block

correct the magnetic sensor (see Sect. 5.2). In this process, the receiver is rotated 360° around each axis of the body coordinates at a fixed position in the space.

Fig. 13 depicts three sensing planes selected during the rotations, each corresponding to a rotation around one axis. The three sensing planes do not really pass through the same position, since the light sensor is not located right at the center of the receiver (in this case the smartphone), and also because of the inaccuracy of manual operation. However, as the receiver is often small in size when compared with the distance to the light source, we can approximately treat the generated sensing planes as passing through the same point.

During the rotation process, the receiver continuously records the RSS when there is a line of sight between the LED lamp and the light sensor. Note that, for each rotation, only a maximum RSS is recorded. Suppose the receiver is located at (x, y, z) and the coordinate (x_j, y_j, z_j) of the j th light source is known, where $x_j > 0$, $y_j > 0$, $z_j > 0$. We have three RSSs and their corresponding normal vectors, the following equations can be established to solve the receiver's position.

$$s_{j,i} = \frac{k_j}{d_j^2} \cdot f_\mu \left(\arccos \left(\frac{d'_{j,i}}{d_j} \right) \right) \cdot f_\omega \left(\arccos \left(\frac{|z - z_j|}{d_j} \right) \right), \quad (4)$$

where $i \in 1, 2, 3$, $j \in 1, 2, \dots, M$, $3 \geq M \geq 1$ denotes the number of different light sources from which the three RSSs are obtained. $s_{j,i}$ means the i th RSS obtained from the j th light source. Note that, $M = 1$ means the three RSSs only obtained from a single light source. The variable $k_j > 0$ is a constant RSS which is measured once for good. The distance from the receiver and the sensing plane to the light sources are

$$d_j = \sqrt{(x - x_j)^2 + (y - y_j)^2 + (z - z_j)^2},$$

and

$$d'_{j,i} = \frac{|A_{j,i}(x - x_j) + B_{j,i}(y - y_j) + C_{j,i}(z - z_j)|}{\sqrt{A_{j,i}^2 + B_{j,i}^2 + C_{j,i}^2}},$$

respectively.

6.1 Solvability of equations

The system of Eq. (4) is a high-order nonlinear one. In general, its properties are not easy to obtain. Fortunately, the solvability of the system of equations relates to the matrix $R = [A_{j,i} \ B_{j,i} \ C_{j,i}]_{3 \times 3}$ consisting of the normal

vectors of the sensing planes from which the three RSSs are generated. The rank of the matrix is $r(R)$. With regard to the solvability of the equations, there are three cases as follows.

1. If $r(R) = 3$, which means there exist at least three linearly independent sensing planes and implies that the three RSSs come from at least one light sources.
2. If $r(R) = 2$, which means there exist at least two linearly independent sensing planes and implies that the three RSSs come from at least two different light sources.
3. If $r(R) = 1$, which means there exist only one sensing plane and implies that the three RSSs come from at least three different light sources. This is the case of the classic Multi-lateral positioning.

According to the analysis above, Eq. (4) has a least square solution.

7 Prototype system

The hardware LiPro consists of two components, the transmitter and the receiver. The transmitter is an off-the-shelf IR LED lamp, with a transmission range of about 7.5 m and an illuminating angle about 130°. This translates to a covered area of about 130 m² on the ground when the lamp is mounted on the ceiling 3 m above the ground. The LED inside the lamp has a power rating of 8 Watts and is attached to an MCU, as shown in Fig. 14(a), (b). To avoid interference between lamps, each LED is assigned two different frequencies, that is, a static subchannel.

At the receiver side, one can use a smartphone such as the Samsung Omnia II GT-I8000 which hosts an IR light sensor. However, the particular implementation of the OS kernel limits the sampling rate of the sensor so is not suitable for our experiments. To exploit the full power of the sensor, we design a specialized sensor module that consists of an ISL29023 light sensor [7] and an LSM303DLH electronic compass. The main board integrates an MCU and a communication module, as shown in Fig. 14(c). The MCU samples the magnetic sensor and the accelerometer at a rate of 20 Hz, and samples the light signal at 800 Hz. The flicker frequency of the LED ranges from 100 to 400 Hz. We evenly divide this range into 20 subchannels with a guard interval of 15 Hz. Hence, a maximum of 10 LEDs are allowed to appear in an overlapped area without interfering with each other, which is more than enough in practice. For example, we can assign the frequencies $f_0 = 100$ and $f_1 = 115$ Hz to the first LED,

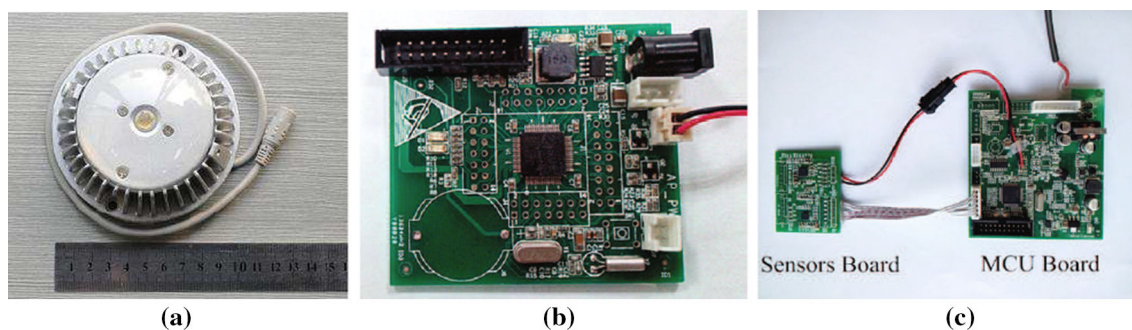
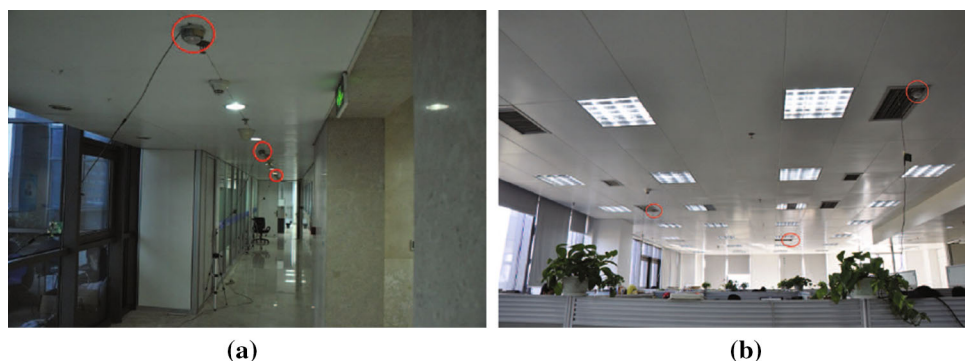


Fig. 14 Hardware design of LiPro. **a** An infrared LED. **b** LED control board. **c** The sensor system

Fig. 15 LED lamps deployed in a corridor and an office area, each with three LED lamps, marked by *red* circles.

a Corridor, **b** office room (Color figure online)



denoted by LED_1 , and frequencies $f_{19} = 385$ and $f_{20} = 400$ Hz to LED_{10} . Note that, to avoid conflict, the third harmonic of frequency should be reserved.

8 Performance evaluation

While we envision that the legacy visible light bulbs can be used as light sources for indoor localization in the future, we currently consider IR LEDs in our experiments as they are invisible and non-intrusive. The experiments are conducted under two typical indoor scenarios: a corridor and an office room. As shown in Fig. 15, we deploy three LEDs in both scenarios. The corridor is of 1.7 m wide and 15 m long, and is free from obstruction. The three LEDs are evenly spaced in a straight line, and we uniformly select 180 positions in the field for testing. The office area measures 8.7 m \times 6.5 m, and contains various types of objects such as cubicles and file cabinets. The three LEDs are mounted on the ceiling, forming a triangle. We uniformly select 60 test points. LiPro is compared with three light-based indoor positioning methods:

1. Epsilon [11]: which follows the classic multilateration method, or requires the user's manual operation depending on application scenarios. As with LiPro, it is based on the Lambertian radiation model [2].

2. RSS weighted average (weighted-Avg): it locates a receiver based on a weighted average of the light sources' locations in sensible range, using light intensities as weights.
3. Coverage: in which the device simply takes the position of the LED lamp producing the highest intensity as its own position. Hence, its positioning accuracy largely depends on the density and placement of the LEDs.

Note that the multilateration method is not applicable in the corridor scenario where the LEDs are deployed linearly.

8.1 Position accuracy

Figure 16 presents the location error of different methods, and Table 1 gives some statistics of errors. For LiPro, the median error is 0.59 and 0.43 m in the corridor and office scenarios, respectively. Epsilon uses the multilateration method in the office room, and requires users' manual operation in the corridor. However, the location error increases by more than two times in the corridor than in the office. This is due to the environmental magnetic interference that causes large errors in heading measurement. LiPro improves the accuracy by two times than weighted-AVG and by four times than the Coverage method in the office scenario. Moreover, in the corridor, LiPro reduces

Fig. 16 CDF of the location error in two scenarios. **a** Corridor, **b** office room

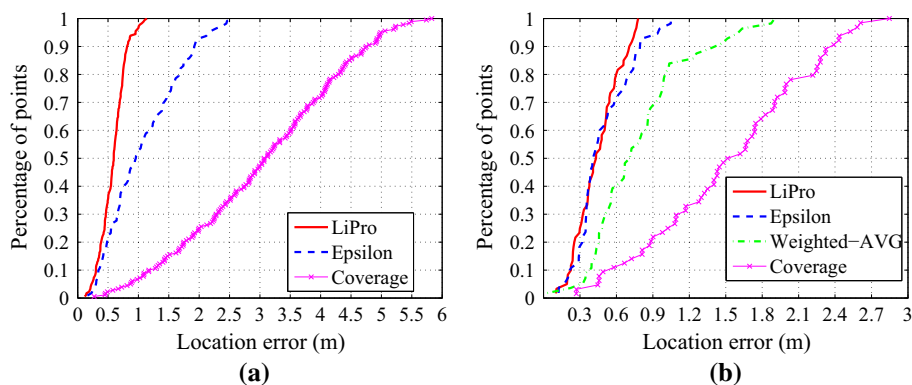


Table 1 Location error statistics of different methods

Test scenario	Method	Error statistics (m)			
		Stdev	Mean	Median	Max
Corridor	LiPro	0.21	0.58	0.59	1.14
	Epsilon	0.61	1.08	0.96	2.54
	Coverage	1.31	3.06	3.10	5.83
Office	LiPro	0.18	0.45	0.43	0.78
	Epsilon	0.23	0.49	0.41	1.05
	Weighted-AVG	0.41	0.79	0.71	1.90
	Coverage	0.66	1.53	1.57	2.85

The bold values emphasize the good performance our technology achieved

the median error and the 90th percentile error by two times than Epsilon, and five times than Coverage, thanks to the calibration of the magnetic sensor.

Compared to the other methods, coverage produces the largest errors in both scenarios, especially in the corridor where it produces errors up to 5.8 m, due to the very rough estimate of the receiver’s position.

8.2 Performance stability

With LiPro, the RSS at the receiver will become lower with the increase of distance between the LED and the device, following an inverse-square law. However, the interference from ambient light sources remains constant. That means a lower signal to noise ratio, which potentially leads to degraded positioning performance.

To study the stability of LiPro, we verify the location error for different distances between the receiver and the closest LED. Generally, the error increases with the distance as shown in Fig. 17. At a reasonable distance, for example 3 m, the location error remains below 0.6 m, which is still acceptable.

We are also interested in how ambient light affects the positioning accuracy. We run the same experiment in

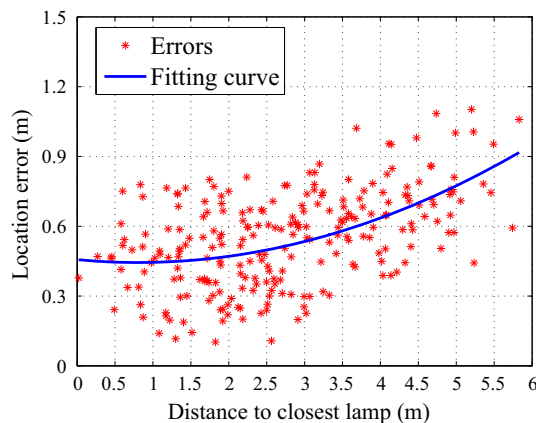


Fig. 17 Location error with respect to the distance to the closest lamp

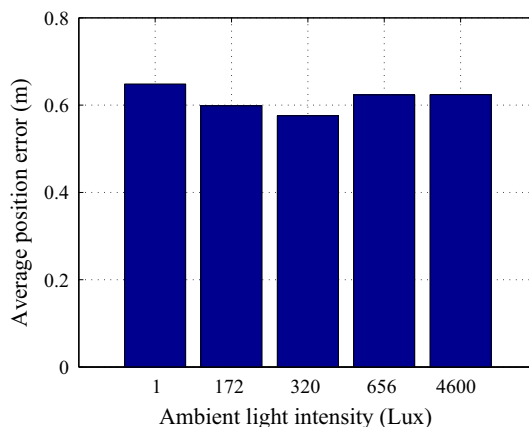


Fig. 18 Location error under ambient light interference

different times of the day with five levels of illuminance (in Lux), i.e., 1, 172, 320, 656, 4600, corresponding to the ambient light intensity at night, in the dusk, in the morning and at noon, respectively, and the 4600 Luxes is measured near the window with sunshine at noon. Figure 18 shows that the variation of ambient light has no noticeable impact on the positioning result.

9 Conclusion

We have proposed the design and implementation of LiPro, a light based indoor positioning method. LiPro uses off-the-shelf LEDs as signal sources as well as location reference points. The receiver continuously measures the light intensity and magnetic field while being rotated by the user. The measurements are then used to solve for the device's position following a rotating multi-face positioning method. The device is able to locate itself with only a single LED light source in sight, which dramatically reduces the system's reliance on light density. Our future work will consider improving the method's applicability in non-line-of-sight scenarios by combining it with RF technology and inertial sensors.

Acknowledgments Guang Tan's work was supported in part by NSFC Grant No. 61379135, Shenzhen Scientific Research Fund No. CXZZ20151117161747567, Shenzhen Overseas High-level Talents Innovation and Entrepreneurship Funds No. KQCX20140520154115 026, Shenzhen Fundamental Research Program under Grant No. JCYJ20140610151856733.

References

- Bahl, P., & Padmanabhan, V. N. (2000). Radar: An inbuilding RF-based user location and tracking system. In *INFOCOM*.
- Barry, J. R. (1994). *Wireless infrared communications* (Vol. 280). Berlin: Springer.
- ByteLight. <http://www.bytelight.com/>.
- Chen, Y., Lymberopoulos, D., Liu, J., & Priyantha, B. (2012). FM-based indoor localization. In *ACM MobiSys*.
- Chintalapudi, K., Iyer, A. P., & Padmanabhan, V. N. (2010). Indoor localization without the pain. In *Mobicom*.
- Chung, J., Donahoe, M., Kim, I., Schmandt, C., Razavi, P., & Wiseman, M. (2011). Indoor location sensing using geo-magnetism. In *MobiSys*.
- Intersil (July 2012). *The ISL29023 datasheet*.
- Kotaru, M., Joshi, K., Bharadia, D., & Katti, S. (2015). Spotfi: Decimeter level localization using wifi. In *SIGCOMM*.
- Kumar, S., Gil, S., Katabi, D., & Rus, D. (2014). Accurate indoor localization with zero start-up cost. In *MOBICOM*.
- Kuo, Y., Pannuto, P., Hsiao, K.-J. & Dutta, P. (2014). Luxapose: Indoor positioning with mobile phones and visible light. In *ACM Mobicom*.
- Li, L., Hu, P., Peng, C., Shen, G., & Zhao, F. (2014). *Epsilon: A visible light based positioning system*. In Proc. NSDI.
- Mariakakis, A. T., Sen, S., Lee, J., & Kim, K.-H. (2014). Sail: Single access point-based indoor localization. In *Proc. of MobiSys*.
- Niculescu, D., & Nath, B. (2003). Ad hoc positioning system (APS) using AOA. In *IEEE INFOCOM*.
- Niculescu, D. & Nath, B. (2004). Vor base stations for indoor 802.11 positioning. In *ACM Mobicom*.
- Nirjon, S., Liu, J., & DeJean, G. (2014). Coin-gps: Indoor localization from direct gps receiving. In *ACM MobiSys*.
- Ozyagcilar, T. (2015). Implementing a tilt-compensated eCompass using accelerometer and magnetometer sensors. In *Free-scale semiconductor*.
- Prince, G. B. & Little, T. D. (2012). A two phase hybrid RSS/ AOA algorithm for indoor device localization using visible light. In *IEEE global communications conference (GLOBECOM)*.
- Priyantha, N. B., Chakraborty, A., & Balakrishnan, H. (2000). The cricket location-support system. In *MobiCom*.
- Rajagopal, N., Lazik, P. & Wowe, A. (2014). Visual light landmarks for mobile devices. In *IPSN*.
- Sahinoglu, Z., Gezici, S., & Guvenc, I. (2008). *Ultra-wideband positioning systems: Theoretical limits, ranging algorithms, and protocols*. Cambridge: Cambridge University Press.
- Sen, S., Choudhury, R. R., & Nelakuditi, S. (2012). Spinloc: Spin once to know your location. In *HotMobile*.
- STMicroelectronics (2010). *Using LSM303DLH for a tilt compensated electronic compass, AN3192 application note*.
- Turner, D., Savage, S. & Snoeren, A. (2011). On the empirical performance of self-calibrating wifi location systems. In *Local computer networks (LCN)*.
- Varshavskya, A., Lara, E. D., Hightower, J., LaMarca, A., & Otsason, V. (2007). Gsm indoor localization. In *Pervasive and mobile computing*.
- Wang, J., Adib, F., Knepper, R., Katabi, D., & Rus, D. (2013) RF-compass: Robot object manipulation using rfids. In *ACM Mobicom*.
- Wang, J., & Katabi, D. (2013). Dude, where's my card?: RFID positioning that works with multipath and non-line of sight. In *Proc. of ACM SIGCOMM*.
- Wu, K., Xiao, J., Yi, Y., Gao, M., & Ni, L. M. (2012) Fila: Fine-grained indoor localization. In *IEEE INFOCOM*.
- Xiong, J., & Jamieson, K. (2013) Arraytrack: A fine-grained indoor location system. In *Usenix NSDI*.
- Yang, L., Chen, Y., Li, X.-Y., Xiao, C., Li, M., & Liu, Y. (2014). Tagoram: Real-time tracking of mobile RFID tags to high precision using cots devices. In *Proc. of Mobicom*.
- Yang, S.-H., Jeong, E.-M., Kim, D.-R., Kim, H.-S., Son, Y.-H., & Han, S.-K. (2013). Indoor three-dimensional location estimation based on led visible light communication. *Electronics Letters*, 49(1), 54–56.
- Yoshino, M., Haruyama, S., & Nakagawa, M. (2008). High-accuracy positioning system using visible led lights and image sensor. In *IEEE radio and wireless symposium*.
- Youssef, M., & Agrawala, A. (2005). The horus wlan location determination system. In *MobiSys*.
- Yun, S., Chen, Y.-C., & Qiu, L. (2015). Turning a mobile device into a mouse in the air. In *MobiSys*.
- Zhou, Z., Kavehrad, M., & Deng, P. (2012). Indoor positioning algorithm using light-emitting diode visible light communications. *Optical Engineering*. doi:10.1117/1.OE.51.8.085009.



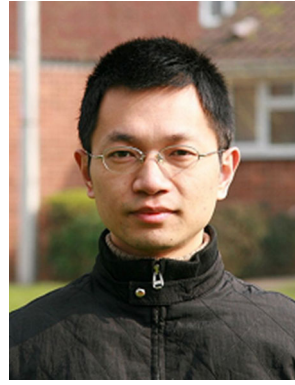
sensor networks.

Bo Xie received the Bachelor's in Software Engineering from Sichuan Normal University in 2007, and Master's degree in Computer Applications Technology from Guangdong University of Technology in 2011. He is currently a Ph.D. student at Shenzhen Institutes of Advanced Technology, Chinese Academy of Sciences (SIAT, CAS), Shenzhen, China. His research interests include indoor localization technology, location-based services and wireless



Shimin Gong (M'15) received the B.S. and M.S. degrees in electrical engineering from Huazhong University of Science and Technology, Wuhan, China, in 2008 and 2012, respectively, and the Ph.D. degree in computer engineering from Nanyang Technological University, Singapore, in 2014. He is currently an Assistant Professor in Shenzhen Institutes of Advanced Technology Chinese Academy of Sciences. He was a Visiting Scholar at The

Chinese University of Hong Kong, Shatin, Hong Kong in 2011, and the University of Waterloo, Waterloo, ON, Canada, in 2012. His research interests include energy harvesting, relaying network, and resource allocation in wireless communications, with a special focus on uncertainty modeling and robust optimization.



Guang Tan is currently a Professor at Shenzhen Institutes of Advanced Technology (SIAT), Chinese Academy of Sciences, China, where he works on mobile computing systems and networks. He received his Ph.D. degree in computer science from the University of Warwick, U.K., in 2007. From 2007 to 2010 he was a postdoctoral researcher at INRIA Rennes, France. His research is sponsored by National Science Foundation of China and Chinese Academy of Sciences. He is a member of IEEE, ACM, and CCF.

Chinese Academy of Sciences. He is a member of IEEE, ACM, and CCF.